American Mineralogist, Volume 104, pages 325–332, 2019

Origin and consequences of non-stoichiometry in iron carbide Fe_7C_3

FENG ZHU[1,*,†], JIE LI[2], DAVID WALKER[3], JIACHAO LIU[4,‡], XIAOJING LAI[5,6], AND DONGZHOU ZHANG[7]

[1]Earth and Environmental Sciences, University of Michigan, Ann Arbor, Michigan 48109, U.S.A. Orcid: 0000-0003-2409-151X
[2]Earth and Environmental Sciences, University of Michigan, Ann Arbor, Michigan 48109, U.S.A. Orcid: 0000-0003-4761-722X
[3]Earth and Environmental Science, LDEO, Columbia University, Palisades, New York 10964, U.S.A.
[4]Earth and Environmental Sciences, University of Michigan, Ann Arbor, Michigan 48109, U.S.A. Orcid: 0000-0001-9676-7473
[5]Hawaii Institute of Geophysics and Planetology, University of Hawaii at Manoa, Honolulu, Hawaii 96822, U.S.A. Orcid: 0000-0003-4451-9421
[6]Department of Geology and Geophysics, University of Hawaii at Manoa, Honolulu, Hawaii 96822, U.S.A.
[7]Hawaii Institute of Geophysics and Planetology, University of Hawaii at Manoa, Honolulu, Hawaii 96822, U.S.A. Orcid: 0000-0002-6679-892X

ABSTRACT

The Eckstrom-Adcock iron carbide, nominally Fe_7C_3, is a potential host of reduced carbon in Earth's mantle and a candidate component of the inner core. Non-stoichiometry in Fe_7C_3 has been observed previously, but the crystal chemistry basis for its origin and influences on the physical properties were not known. Here we report chemical and structural analyses of synthetic Fe_7C_3 that was grown through a diffusive reaction between iron and graphite and contained 31 to 35 at% carbon. We found that more carbon-rich Fe_7C_3 has smaller unit-cell volume, suggesting that excess carbon atoms substituted for iron atoms instead of entering the interstitial sites of closed-packed iron lattice as in FeC_x steel. Carbon may be the lightest alloying element to substitute for iron. The substitution leads to a larger reduction in the unit-cell mass than the volume so that the carbon-rich end-member may be as much as 5% less dense than stoichiometric Fe_7C_3. If Fe_7C_3 solidifies from Earth's iron-rich liquid core, it is expected to have a nearly stoichiometric composition with a compositional expansion coefficient of ~1.0. However, laboratory experiments using carbon-rich synthetic Fe_7C_3 to model the inner core may overestimate the amount of carbon that is needed to account for the core density deficit.

Keywords: Iron carbide, non-stoichiometry, substitution, interstice, light element, density deficit, compositional expansion coefficient; Physics and Chemistry of Earth's Deep Mantle and Core

INTRODUCTION

Eckstrom-Adcock iron carbide (Fe_7C_3) was first discovered in a hydrocarbon synthesis plant (Eckstrom and Adcock 1950). Fe_7C_3 is considered a potential host of reduced carbon in Earth's deep mantle, where metallic iron is expected to be stable (Rohrbach and Schmidt 2011). It is also a candidate component to explain the density deficit and anomalously low shear wave velocity of the inner core (Chen et al. 2012, 2014; Prescher et al. 2015; Liu et al. 2016). M_7C_3 (M_2C)-type intermediate transition-metal carbides have been found as inclusions in superdeep diamonds together with cementite M_3C, where M stands for Fe, Co, Ni, Cr, and Mn. These natural M_7C_3 (M_2C) and M_3C samples can have ~6–8 at% C content variation in the same structure. (Kaminsky and Wirth 2011; Smith et al. 2016). Synthetic iron carbides also show considerable compositional variation, ranging from 29 to 36 at% carbon in Fe_7C_3 and from 17 to 31 at% carbon in Fe_3C (Buono et al. 2013; Walker et al. 2013). Deviation from stoichiometric composition led to a reduction of the Curie temperature of Fe_3C (Walker et al. 2015). Moreover, a carbon-poor Fe_3C was found to have a smaller unit-cell volume than a slightly carbon-rich phase, suggesting that the carbon deficiency originates from carbon vacancy. The correlation between volume and composition is similar to FeC_x or FeH_x alloys, where unit-cell volume increases with the increasing amount of light element, and opposite to Fe-O, Fe-Si, and Fe-S alloys where the unit-cell volume decreases with the increasing amount of light element (Table 1). On the other hand, the origin and effects of non-stoichiometry on Fe_7C_3 are still not known. Here we investigate the composition and structure of non-stoichiometry in Fe_7C_3 through synchrotron X-ray diffraction (XRD) and electron probe microanalysis (EPMA), and we discuss the implications for the stability and properties of carbides in the deep Earth.

METHODS

Non-stoichiometric iron carbide Fe_7C_3 was synthesized using a multi-anvil apparatus at the Lamont-Doherty Earth Observatory (LDEO serial BB-1233) (Walker et al. 2013). The starting material consists of a 250 μm thick iron disk (Goodfellow hard iron foil, >99.5%) sandwiched between two graphite cylinders (National Carbon Spectroscopic grade graphite), surrounded by high-purity MgO sleeve. The sample was contained in an 8 mm truncated edge length (TEL) octahedron of Ceramacast 584 castable ceramic (Aremco) and equilibrated at 7 GPa (350 U.S. tons from oil pressure) and 1300 °C for 19 h. The temperature difference across the sample is estimated to be <10 °C, and the pressure uncertainty is estimated to be 0.5 GPa in the sample capsule. The experimental product was ground to form a 1.8 mm long, 0.4 mm tall, and 300 μm thick pellet (parallel to the rotation axis of the original Fe disk and C cylinders) that presented as a sectioned sandwich with carbide as the jelly between carbon bread slices for synchrotron XRD measurements at 13-BM-C of the Advanced Photon Source

* E-mail: fzhuum@umich.edu
† Special collection papers can be found online at http://www.minsocam.org/MSA/AmMin/special-collections.html.
‡ Present address: Department of Geological Sciences, Jackson School of Geosciences, University of Texas at Austin, Austin, TX, 78712, U.S.A.

0003-004X/19/0003–325$05.00/DOI: https://doi.org/10.2138/am-2019-6672

TABLE 1. Density of iron-light-element alloys at 1 bar and 300 K

	Z	Light element (wt%)	Light element (at%)	Cell volume (Å^3)	Cell mass (g/mol)	Mechanism	Density (g/cm^3)	α_c[a] (% per wt%)	α_c*[b] (% per wt%)
α-Fe[c]	2	0	0	23.54	112	–	7.90		
γ-Fe[d]	4	0	0	44.83	224	–	8.30		
ε-Fe[e]	2	0	0	22.49	112	–	8.27		
γ-FeC_x[d]	4	0.4	1.2	45.65	224.96	C interstice	8.183	2.5	1.4
		1.8	8	47.24	228.18	C interstice	8.020	1.7	
Fe_3C[f] ($FeC_{0.33\pm x}$)	4	5.8	22.3	154.39	713.33	C vacancy	7.672	1.3	–0.9
		6.7	25		720	assume stoichiometry[k]	7.744	1.1	
		6.9	25.6	154.73	714.14	substitution	7.664	1.1	
		6.7	25		720	assume stoichiometry[k]	7.727	0.96	
Fe_7C_3[g] ($FeC_{0.43\pm x}$)	2	8.8	31	186.8(1)	847.32	substitution	7.532	1.0	2.6
		8.4	30		856	assume stoichiometry[k]	7.610	0.93	
		10.3	35	186.2(1)	812.17	substitution	7.243	1.2	
		8.4	30		856	assume stoichiometry[k]	7.634	0.74	
$Fe_{1-x}O$[h]	4	23.1	51.3	79.95	276.8	Fe vacancy	5.749	1.3	2.1
		23.7	52.1	78.95	270.08	Fe vacancy	5.681	1.3	
$Fe_{1-x}Si_x$[i]	2	5.2	10	22.99	106.4	substitution	7.684	1.4	0.4
		8.1	15	22.63	103.6	substitution	7.601	1.0	
$Fe_{1-x}S$[j]	2	36.4	50	60.36	176	stoichiometric	4.840	1.1	
		38.6	52.4	59.27	166.7	Fe vacancy	4.670	1.1	1.6
		39.5	53.3	57.98	162	Fe vacancy	4.640	1.1	1.3

[a] Compositional expansion coefficient with respect to ε-Fe.
[b] Relative compositional expansion coefficient between two compositions with same phase. The $Fe_{1-x}S$ was calculated based on the stoichiometric FeS with 50 at% S.
[c] Hull (1917).
[d] Okamoto (1992).The density of γ-Fe at 300 K was extrapolated from data at high temperature, where it is stable.
[e] Fei et al. (2016). The density of ε-Fe was extrapolated from data at high pressure, where it is stable.
[f] Walker et al. (2013).
[g] This study.
[h] Hazen and Jeanloz (1984).
[i] Machová and Kadečková (1977) and Routbort et al. (1971).
[j] Koto et al. (1975) and Nakano et al. (1979).
[k] Incorrect density calculation using unit-cell mass from stoichiometric formula and unit-cell volume from non-stoichiometric sample.

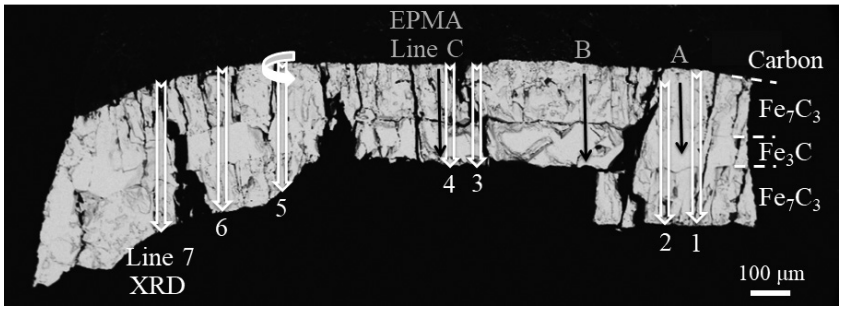

FIGURE 1. Backscattered electron (BSE) image of the diffusive reaction product consisting of two layers of Fe_7C_3 (gray), each sandwiched between graphite (C, dark) and Fe_3C (light gray). The white and black arrows mark the positions of the XRD and EPMA line scans analyses, respectively. The sample was rotated around the stacking direction of the sandwich, as indicated by the curved arrow.

(APS), Argonne National Laboratory (ANL). The X-ray wavelength is 0.4340 (±2 × 10^{-5}) Å and the beam size is 12 μm × 18 μm at the full-width at half maximum (FWHM) (horizontal×vertical direction in Fig. 1). The sample to detector distance is 164.10 (±0.03) mm. The slice was rotated around the original rotation axis of the Fe disk and C cylinders (stacking direction of the sandwich) by ±30° to reduce the effect of preferred orientation in the coarse-grained sample. The XRD data were processed using Dioptas (Prescher and Prakapenka 2015) and PDIndexer (Seto et al. 2010) software.

After the XRD measurements, the slice was coated with aluminum for electron microprobe analysis, using the JOEL-7800FLV scanning electron microscope (SEM) and Cameca SX100 EPMA at the Electron Microbeam Analysis Laboratory (EMAL) of University of Michigan. No chemical contamination was detected in the SEM and EPMA measurements. For the EPMA analysis, an 11 kV accelerating voltage and a 70 nA beam focused to ~1 μm diameter was used to obtain compositional data (Dasgupta and Walker 2008). The penetration depth of the beam was estimated to be <20 μm. Pure Fe and synthetic stoichiometric Fe_3C were used as the standards (Liu et al. 2016). The measurement time for the sample was 10 s on the peak positions and 5 s on the background.

RESULTS AND DISCUSSION

Anti-correlation between unit-cell volume and carbon content in non-stoichiometric Fe_7C_3

Backscattered electron (BSE) image showed that the synthesis experiment produced two layers of the Eckstrom-Adcock carbide, nominally Fe_7C_3, each sandwiched between a layer of cementite, nominally Fe_3C, in the center of the sample and unreacted carbon on both ends (Fig. 1). The layered structure indicates that the C and Fe_3C layers were not fully equilibrated when the sample was quenched from high temperature. As a result, ongoing C diffusion from the C layers to Fe_3C layer through the Fe_7C_3 layers in between was preserved in the sample, creating the gradient of C content in the Fe_7C_3 layers, which points from the carbon-rich end near the Fe_7C_3/C boundary to carbon-poor end near the Fe_7C_3/Fe_3C boundary.

The layered distribution of the three phases was confirmed by XRD line scans (Fig. 2). The phase assemblies evolve from C+Fe_7C_3 at the graphite ends to Fe_7C_3 and then to Fe_3C. Some XRD patterns of the Fe_7C_3 contained variable amounts of Fe_3C. Minor Fe_7C_3 phase was also found in the XRD collected from the Fe_3C band. The occurrence of both carbides in the XRD patterns collected from the interior of different bands appears inconsistent with the clear separation of the bands in the BSE and optical images. We found that on the exiting side of the X-ray beam the center Fe_3C band is 40 μm thinner, suggesting that the boundaries between Fe_7C_3 and Fe_3C are not parallel and therefore the beam that enters the sample near the interface would traverse both phases. This effect is enhanced considering that 25% of X-ray intensity is outside the FWHM and can produce diffraction signals from 40 μm areas. It is also possible that the stacking direction of the sample is slightly tilted toward or away from the X-ray beam direction and therefore XRD patterns containing single carbide are only collected from measurements near the center of each band, as we observed.

Despite these complications, a unit-cell volume composite map constructed from the XRD line scans revealed a general trend that Fe_7C_3 closer to the carbon layer has a smaller unit-cell volume (Fig. 3). We used a hexagonal structure ($P6_3mc$) (Herbstein and Snyman 1964) to refine the structure of Fe_7C_3 since it better explained the observed patterns. Six fixed peaks of (112), (031), (022), (220), (033), and (232) that have no overlap with Fe_3C strong peaks were used for the refinement of all present unit-cell volumes to avoid complications, and the largest unit cell of Fe_7C_3 was found in the Fe_3C center band, where Fe_7C_3 occurred as a minor phase in the mixed XRD patterns. The trend of decreasing volume toward the carbon layer is further confirmed by the stacked XRD patterns showing a systematic shift of peak position toward larger 2θ as the X-ray beam moved from the Fe_3C-Fe_7C_3 boundary toward the Fe_7C_3-C boundary (Fig. 4). Fe_3C exhibits a similar correlation of higher carbon content with smaller unit-cell volume, although there is considerable scatter and the trend is not as well resolved (Figs. 4a and 4d). These peak shifts, although only ~0.02°, are much larger than the potential shifts caused by uncertainties in X-ray wavelength (0.0006° at 2θ ~14° corresponding to 1 eV energy fluctuation) and sample-to-detector distance (0.0024° at 2θ ~14° corresponding to 30 μm sample distance variation). The sample-detector distance at the center band of Fe_3C+Fe_7C_3 mixture can differ by up to ~100 μm from the Fe_7C_3 band at the edge. Accordingly, the 2θ could shift up to 0.008° and may have a visible influence on the unit-cell volumes of the center-most Fe_7C_3, but not enough to account for the total observed shift. Additionally, the peak shift was observed in Fe_7C_3 phase at the edge free of Fe_3C (Fig. 4c), thus ruling out the possibility that the 2θ shift mainly comes from phase mixture. In all seven line scans the largest volumes appear in the center, suggesting that the 2θ shift does not come from random fluctuation. Therefore, the variation in cell volume suggests non-stoichiometry in Fe_3C and Fe_7C_3. More importantly, the data suggest an anti-correlation between cell volume and carbon content: As the carbon concentration increases, the cell volume became smaller.

EPMA line scans showed two clusters of composition at ~24–27 at% and ~31–35 at% carbon, corresponding to Fe_3C and Fe_7C_3, respectively (Fig. 5). The ranges of non-stoichiometry agree with the previous studies (Buono et al. 2013; Walker et al. 2013). The compositions of Fe_3C mostly fell on the carbon-rich side of the stoichiometric compound, consistent with the fact that the iron in the starting material was fully consumed and the product still contains unreacted carbon. Overall the carbon content decreases from the region next to unreacted carbon toward that next to the Fe_3C band, consistent with the direction of C diffusion (Fig. 5). Compositional fluctuation exists in individual line scan, especially Line A near the distal edge, due to the complexity in carbon diffusion (Walker et al. 2013) and the large uncertainty in measuring C concentration by EPMA.

Compared with EPMA measurements, less fluctuation of the unit-cell volume was observed in XRD (Figs. 3 and 5). This is mainly because the sample volume covered by XRD is significantly larger than that by EPMA (12 × 18 μm beam size and 300 μm depth in XRD compared with ~1 μm beam size and <20 μm penetration depth in EPMA). With thousands of times volume coverage, together with the sample rotation, the XRD measurements effectively reduced the scattering caused by the

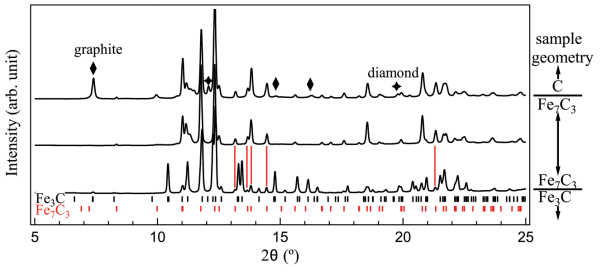

FIGURE 2. Representative XRD patterns collected during line scan. The pattern of the center Fe_3C band (lower) contains a minor amount of Fe_7C_3. The interior of the Fe_7C_3 band (middle) is pure phase. Diamond, graphite, and Fe_7C_3 are found in the upper pattern collected from the C/Fe_7C_3 boundary. (Color online.)

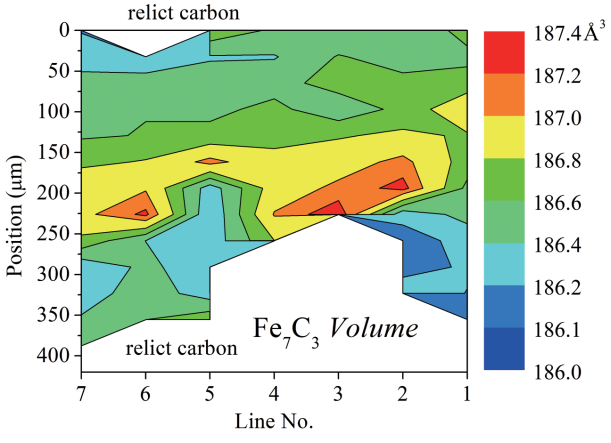

FIGURE 3. Composite map constructed from seven line scans at 30 μm step. The largest unit-cell volume of Fe_7C_3 was found in the center of the sample where Fe_7C_3 co-exists with Fe_3C. The smallest volume is near the edge where Fe_7C_3 phase coexists with unreacted carbon. The Fe_7C_3 in the center may have C concentration lower than 31 at%. (Color online.)

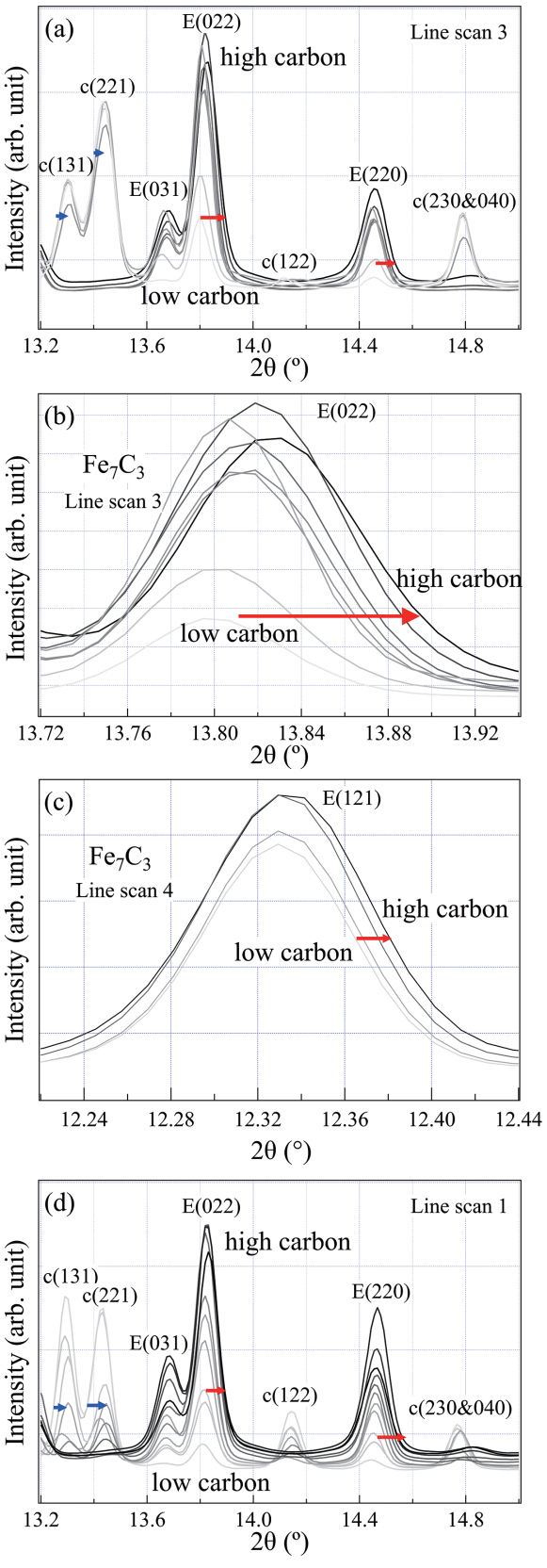

◀**FIGURE 4.** Stacked XRD patterns from line scans. (**a**) Overall patterns showing that as the X-ray beam moved toward carbon-rich areas, the Fe_7C_3 peaks grew at the expense of the Fe_3C peaks, and both Fe_7C_3 and Fe_3C peaks shifted to higher 2θ (blue and red arrows). (**b**) The Fe_7C_3 (022) peaks in a series of XRD patterns collected from C-Fe_7C_3 interface (black, high carbon) to Fe_7C_3-Fe_3C interface (light gray, low carbon content). (**c**) The Fe_7C_3 (121) peaks in several XRD patterns collected from the interior of the Fe_7C_3 layer free of Fe_3C peaks shifted to higher 2θ as the carbon content increased. (**d**) Overall patterns of Line 1 at the distant edge, where the variation of carbon content is less than that in the central positions. Both Fe_7C_3 and Fe_3C peaks still shifted to higher 2θ as the X-ray beam moved toward carbon-rich areas. (Color online.)

complexity of local composition and obtained the average lattice parameters for the covered volume.

From the most carbon-rich part with 35 at% carbon to the least carbon-rich part with 31 at% carbon in the Fe_7C_3 band, the unit-cell volume expands by ~0.3% from ~186.2 to 186.8 Å^3. Larger unit-cell volume up to ~187.4 Å^3 was obtained from the Fe_7C_3-Fe_3C mixture in the center band, where carbon content may be lower than 31 at% and the XRD beam averaged less volume from carbon-rich Fe_7C_3 when it crossed the Fe_7C_3-Fe_3C phase boundary. Because large uncertainty may exist in both the composition and volume refinement in this phase mixture region, it is excluded from the latter density calculation.

Origin of non-stoichiometry in Fe_7C_3 and Fe_3C

The composition-volume relation of iron carbides can be used to infer the mechanism by which carbon is removed or added from the structures of stoichiometric compounds. Cementite Fe_3C is usually considered an interstitial alloy in which carbon atoms adopt the sixfold interstitial sites of iron in *hcp* structure (Barrett 1943; Scott et al. 2001). First-principles calculations found that carbon enters the interstitial sites of closed packed structure of iron and therefore adding a small amount of carbon ($x < 0.1$) to *hcp* Fe expands the lattice (Caracas 2017). The interstitial model, however, cannot explain the smaller volumes of carbon-rich Fe_7C_3 and Fe_3C, suggesting that carbon-iron substitution may be the cause of carbon-rich carbides.

By contrast, Walker et al. (2013) found that the unit-cell volume of a carbon-poor Fe_3C with 22.3 at% carbon is smaller than that of a slightly carbon-rich Fe_3C with 25.6 at% carbon. Petch (1944) also found that volume decreases with decreasing C content in Fe-saturated cementites as they become less stoichiometric and C-poorer with rising temperature. Results from the two literature studies on C-poor cementite, compared to the present study of C-rich cementite, therefore, suggest that deviation from the stoichiometric composition of Fe_3C in either direction reduces the cell volume and that the mechanisms of non-stoichiometry may be different on different sides of stoichiometric Fe_3C. In light of this new evidence, the supposition of Walker et al. (2015) that the non-stoichiometry mechanism on the C-rich side of Fe_3C is interstitial is less plausible than that it is substitutional. Walker et al. (2015) found that the Curie temperature is lower on either side of Fe_3C, but the rate of T_c reduction on the C-rich side is twice that on the C-poor side. They attributed the rate differences to larger configurational entropy production by interstitial C on the C-rich side than by C vacancy on the C-poor side. We now regard substitutional C as a more plausible mechanism on the

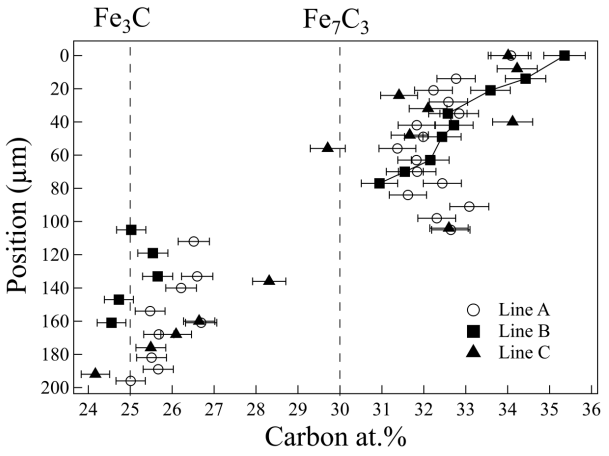

FIGURE 5. EPMA line scans showing compositional variations in Fe_3C and Fe_7C_3 and carbon gradient in Fe_7C_3. Line A in the distal edge has less variation than Line C in the central position, consistent with Walker et al. (2013).

C-rich side on the basis of the new evidence presented here. The entropy argument, however, remains unchanged because there are still twice as many sites for substitution on the C-rich side as there are for C vacancy on the C-poor side of Fe_3C. The entropy production rate in this particular case is insensitive to compositional variation mechanism for introducing C richness.

A closer look at the structures of Fe_3C and Fe_7C_3 reveal that carbon takes a distinct eightfold square antiprism site instead of the interstitial sites of the close-packed iron lattice (Fig. 6). The presence of carbon distorts the sixfold interstitial sites and enlarges the lattice. As a result, 2/3 of the iron atoms in Fe_3C and 6/7 of those in Fe_7C_3 have only 11 nearest iron neighbors and the sub-structures of iron atoms are no longer ideal *hcp* closest packing. The eightfold carbon sites and 11-fold iron sites in the carbide structures can be explained by the nature of metallic bonding between carbon and iron, where carbon acts as an electron donor and enhances the hybridization between the partially filled 3d orbital and the 4s orbital of iron (Goldschmidt 1967). As a result, C in iron carbides should be treated as C^0, instead of C^{4-} as in covalent and stoichiometric compounds such as SiC, Al_4C_3, and Mg_2C. For metallic bonding between Fe^0 and C^0 the radius ratio r_C/r_{Fe} is ~0.62 or slightly larger with corrections for electronegativity of Fe (1.83) and C (2.55) (Allred 1961). According to Pauling's rules this ratio is slightly too high for carbon to take the sixfold interstitial site ($r_A/r_X = 0.414$) and too low for C-Fe substitution ($r_A/r_X = 1$). Consequently, only a small amount of interstitial carbon is allowed in FeC_x alloys. Carbon in Fe_3C and Fe_7C_3 adopts eightfold square antiprism sites ($r_c/r_a = 0.645$ in Pauling's rules) instead of entering the interstices of close-packed iron.

Because carbon adopts an eightfold site that is not much smaller than 11-fold iron sites, excess carbon atoms in Fe_3C and Fe_7C_3 may be incorporated into the structure through substitution of carbon for iron (Fig. 6). This substitution explains the reduced volumes of carbon-rich Fe_3C and Fe_7C_3. No carbon-poor Fe_7C_3 has been found in this study or previous synthesis (Walker et al. 2013), suggesting that it is less stable than a two-phase mixture

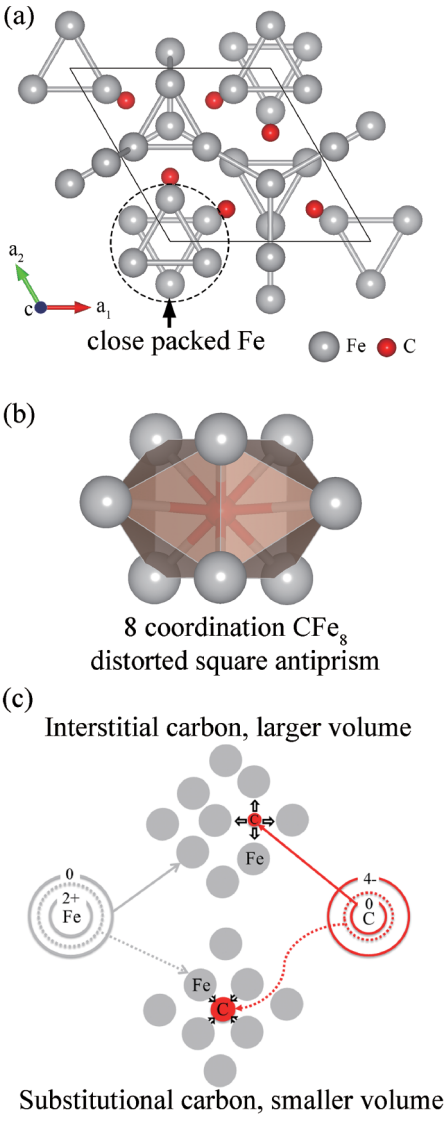

FIGURE 6. (**a**) Structure model of Fe_7C_3 ($P6_3mc$) with locally close-packed iron atoms (dashed circle); (**b**) CFe_8 polyhedron, which can be viewed as a distorted square antiprism with a rhombus in front of a rectangle; (**c**) interstitial carbon in Fe lattice (upper) and C-Fe substitution (lower). The Pauling-Ahrens radii of Fe^0, Fe^{2+}, and C^0 are from Ahrens (1952) and Pauling (1960). The radius of C^{4-} is calculated from linear extrapolation of the radii of O^{2-} and N^{3-}. The dashed circles represent the radii of Fe^0 and C^0 scaled to the electronegativity of Fe and C at 2.55 and 1.83, respectively. (Color online.)

of Fe_3C and stoichiometric Fe_7C_3.

The inferred origin of non-stoichiometry in carbon-poor and carbon-rich Fe_3C is consistent with the relations between the lattice parameters and carbon content. An anti-correlation in lattice parameters was reported in C-poor Fe_3C such that the *b* axis elongates with decreased C content while the unit-cell volume (and *a*, *c* axes) shrinks (Petch 1944; Walker et al. 2013). This kind of anti-correlation was not observed in the C-rich Fe_3C in this study. For example, in Line 1 the maximum unit-cell volume of Fe_3C is 155.93(27) Å^3 with $a = 5.098(2)$ Å, $b = 6.760(4)$ Å, and *c*

= 4.525(2) Å, and the minimum unit-cell volume is 155.47(38) Å^3 with a = 5.094(2) Å, b = 6.748(7) Å, and c = 4.523(3) Å. Carbon in the antiprism site of Fe_3C introduces pleats to the close-packed Fe in b direction, which changes the folding angle of the pleats from 180° (no folding) to ~120°. The carbon vacancy unbends the pleats in the b direction and lets them stack better in a and c direction, thus increasing the axial length in the b direction and decreasing it in the a/c direction. On the C-rich side, all the antiprism sites are filled and the excess carbon takes the Fe site instead. Because there is no further occupancy of the antiprism sites, the anti-correlation between b and unit-cell volume disappears on the C-rich side.

The inferred site occupancy is further corroborated by the diffusion rates of carbon and iron in FeC_x alloy and iron carbides. Carbon diffusion in austenite and ferrite is considered a typical example of rapid interstitial diffusion, whereas self-diffusion of iron is a typical example of substitution (vacancy) diffusion. At 1 bar and 1000 K, the diffusion coefficient of carbon in Fe_3C is ~10^{-15} m^2/s, which falls between that of carbon in *bcc* Fe (~10^{-10} m^2/s) or *fcc* Fe (~10^{-12} m^2/s) and that of iron in *bcc* Fe (~10^{-17} m^2/s) or *fcc* Fe (~10^{-19} m^2/s) (Ozturk et al. 1984; Gale and Totemeier 2003; Hillert et al. 2005). The intermediate value of diffusion coefficient suggests that carbon in Fe_3C cannot be treated as an interstitial constituent. Molecular dynamics simulations suggest that sixfold interstitial sites may serve as transient "stepping stones" to facilitate diffusion of carbon among antiprismatic sites (Levchenko et al. 2009). This interstice-assisted diffusion mechanism implies carbon diffusion in Fe_3C may include both interstitial and substitutional mechanism, and the substitutional diffusion is likely the rate-limiting step that caused the observed gradient non-stoichiometry in the diffusive reaction product in this study.

The roughly planar boundaries between Fe_3C, Fe_7C_3, and C in the recovered samples synthesized at 7 GPa from this and a previous study suggested that the reactions were controlled mainly by lattice diffusion, without significant transport along grain boundaries (Walker et al. 2013). The widths of the Fe_3C layer and the Fe_7C_3 layer in either this study or the previous study are comparable, thus indicating the lattice diffusion rates of carbon in Fe_7C_3 and Fe_3C are similar, which in turn implies the same origin of non-stoichiometry on the carbon-rich sides of these carbides.

Density of non-stoichiometric iron-light-element alloys

The density of an iron carbide may be calculated from its unit-cell volume from XRD measurements and the composition as determined by microprobe analysis only if we can infer the mechanism of non-stoichiometry. For a carbon-rich Fe_7C_3 with 35 at% carbon, the formula unit may be written as $Fe_{6.5}C_{3.5}$ for a substitution alloy or $Fe_7C_{3.77}$ for an interstitial alloy. Depending on the mechanism of non-stoichiometry, the calculated densities for the same unit-cell volume and chemical composition could differ by more than 5% (Table 1). It is therefore important to understand the nature of non-stoichiometry.

The presence of a light element in an iron-alloy usually reduces its density. The efficiency of density reduction can be described by the compositional expansion coefficient α_c, the ratio between the relative density reduction and the concentration of the light element in weight percent. With respect to *hcp* iron, the α_c of stoichiometric Fe_3C and Fe_7C_3 is 1.4, corresponding to 1.4% density reduction for 1 wt% of carbon in the Fe-alloy (Fig. 7). Carbon excess in Fe_7C_3 leads to a local excursion of α_c to 2.6, because replacing iron with carbon reduces the cell mass much more than the cell volume. It is interesting to note that carbon vacancy in Fe_3C may give rise to local negative α_c with respect to stoichiometric composition: Between carbon-poor Fe_3C with vacancy and nearly stoichiometric Fe_3C, the local α_c is –0.9 (Fig. 7, Table 1).

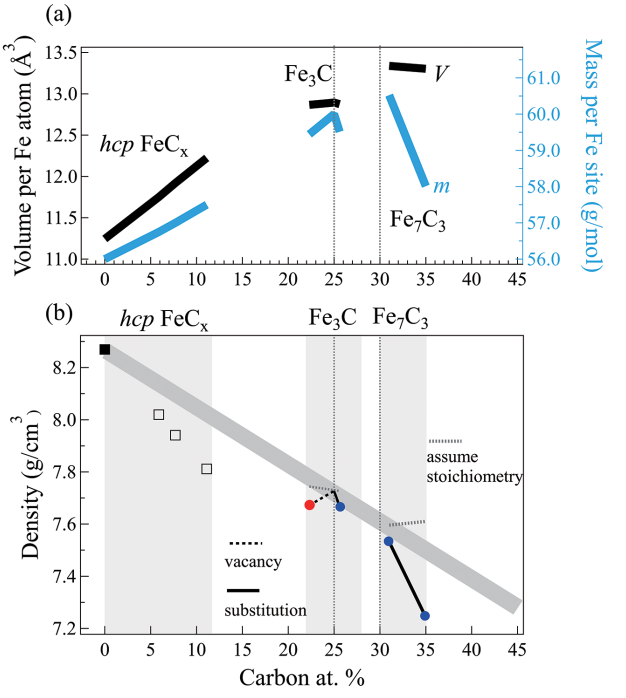

FIGURE 7. The (**a**) volume and mass per iron atom, and (**b**) density of FeC_x, Fe_3C, and Fe_7C_3 as a function of carbon content. In **b**, the gray line is drawn through pure *hcp* Fe and stoichiometric Fe_3C. The dotted lines represent densities calculated by assuming stoichiometric composition. The dashed and solid lines correspond to the densities calculated by applying the carbon vacancy or C-Fe substitution mechanism, respectively. (Color online.)

Non-stoichiometry is common among iron-light-element alloys and may cause variations in compositional expansion coefficient (Fig. 8). At ambient conditions, however, the complexity in calculating density from measured cell volume and composition may be applicable to carbon alone. This is because the atomic or covalent radius of carbon makes a borderline case for it to act as an interstitial constituent as in FeC_x, or as a substituent of iron as in carbon-rich Fe_3C and Fe_7C_3. With r_H/r_{Fe} ~0.29, FeH_x is considered a typical interstitial alloy. Silicon is comparable to iron in size (r_{Si}/r_{Fe} ~0.94) and electronegativity and therefore all Fe-Si alloys are substitutional. Oxygen and sulfur are highly electro-negative and their anions are much larger than an iron cation, and therefore iron vacancy is the dominant mechanism for non-stoichiometry in $Fe_{1-x}O$ (Hazen and Jeanloz 1984) and $Fe_{1-x}S$ (Palache et al. 1944). At high pressures, $Fe_{1-x}S_x$ ($x < 0.1$) solutions have been predicted and observed (Li et al. 2001; Alfe

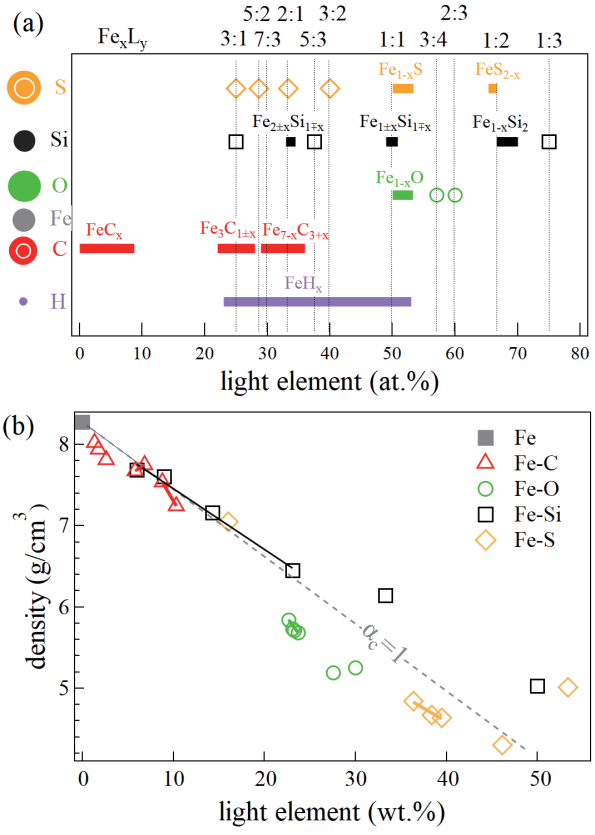

Figure 8. (**a**) Non-stoichiometry in iron-light-element alloys. Open symbols represent stoichiometric compounds. The radii of light elements and iron are represented by the circles on the left. The radius of C^{4-} or S^{2-} (outer circles) is larger than that of C^0 or S^0 (inner circles), respectively. (**b**) Density of iron-light-element alloys as a function of light element concentration. The ranges of non-stoichiometric compositions are denoted by horizontal bars. (Color online.)

et al. 2002; Kamada et al. 2010; Kamada et al. 2012). Pressure may influence the electronegativity and radii of iron and sulfur differently, hence it may be necessary to examine the dissolution mechanism of sulfur in iron to correctly calculate the density of Fe-S alloys at high pressures.

Implications

As a candidate component of the Earth's inner core, Fe_7C_3 is likely nearly stoichiometric because it solidifies from the outer core that contains at least 85 wt% iron. In recent mineral physics experiments, Fe_7C_3 samples are often synthesized in graphite capsules and therefore carbon-saturated (Nakajima et al. 2011; Chen et al. 2014; Prescher et al. 2015). In these studies, the density of Fe_7C_3 was calculated by assuming stoichiometric composition because non-stoichiometry was not widely recognized at the time, and the exact compositions of micrometer-sized samples used for the diamond-anvil cell measurements were not readily accessible. The calculated density of synthetic C-rich Fe_7C_3 could be as much as 1.2% larger than nearly stoichiometric Fe_7C_3 in the core, and therefore, the mass fraction of Fe_7C_3 that is needed to account for the density deficit of the inner core was likely overestimated by ~6%.

The above discussion assumes that the range of non-stoichiometry in Fe_7C_3 determined here at 7 GPa and 1300 °C applies at deep mantle or inner core conditions. The higher temperatures in the deep mantle likely make possible larger deviations from stoichiometry (Buono et al. 2013; Walker et al. 2013). Pressure and/or temperature induced exchanges in the compositions of non-stoichiometric iron carbides may lead to consumption or production of diamonds during downwelling or upwelling processes and influence chemical equilibrium in deep Earth.

Non-stoichiometry is common in iron-rich alloys and may influence the density, sound velocity, and other physical properties. Further studies are needed to quantify the effects of pressure and temperature on non-stoichiometry of iron-rich alloys at relevant conditions and explore the implications for the light element composition of the core.

Funding

The XRD experiment was performed at GeoSoilEnviroCARS (The University of Chicago, Sector 13), Advanced Photon Source (APS), Argonne National Laboratory. GeoSoilEnviroCARS is supported by the National Science Foundation (NSF), Earth Sciences (EAR-1634415), and Department of Energy (DOE), GeoSciences (DE-FG02-94ER14466). This research used resources of APS, a U.S. DOE Office of Science User Facility operated for the DOE Office of Science by Argonne National Laboratory under Contract No. DE-AC02-06CH11357. This work was partially supported by Sloan Foundation Deep Carbon Observatory Grant G-2017-9954, NSF EAR 1763189, and NSF AST 1344133.

References Cited

Ahrens, L.H. (1952) The use of ionization potentials Part 1. Ionic radii of the elements. Geochimica et cosmochimica Acta, 2(3), 155–169.
Alfe, D., Gillan, M., and Price, G. (2002) Ab initio chemical potentials of solid and liquid solutions and the chemistry of the Earth's core. The Journal of Chemical Physics, 116(16), 7127–7136.
Allred, A. (1961) Electronegativity values from thermochemical data. Journal of Inorganic and Nuclear Chemistry, 17(3-4), 215–221.
Barrett, C.S. (1943) Structure of Metals. McGraw-Hill, New York.
Buono, A.S., Dasgupta, R., Lee, C.-T.A., and Walker, D. (2013) Siderophile element partitioning between cohenite and liquid in the Fe–Ni–S–C system and implications for geochemistry of planetary cores and mantles. Geochimica et Cosmochimica Acta, 120, 239–250.
Caracas, R. (2017) The influence of carbon on the seismic properties of solid iron. Geophysical Research Letters, 44(1), 128–134.
Chen, B., Gao, L., Lavina, B., Dera, P., Alp, E.E., Zhao, J., and Li, J. (2012) Magneto-elastic coupling in compressed Fe_7C_3 supports carbon in Earth's inner core. Geophysical Research Letters, 39(18).
Chen, B., Li, Z., Zhang, D., Liu, J., Hu, M.Y., Zhao, J., Bi, W., Alp, E.E., Xiao, Y., and Chow, P. (2014) Hidden carbon in Earth's inner core revealed by shear softening in dense Fe_7C_3. Proceedings of the National Academy of Sciences, 111(50), 17755–17758.
Dasgupta, R., and Walker, D. (2008) Carbon solubility in core melts in a shallow magma ocean environment and distribution of carbon between the Earth's core and the mantle. Geochimica et Cosmochimica Acta, 72(18), 4627–4641.
Eckstrom, H.C., and Adcock, W.A. (1950) A new iron carbide in hydrocarbon synthesis catalysts. Journal of the American Chemical Society, 72(2), 1042–1043.
Fei, Y., Murphy, C., Shibazaki, Y., Shahar, A., and Huang, H. (2016) Thermal equation of state of hcp-iron: Constraint on the density deficit of Earth's solid inner core. Geophysical Research Letters, 43(13), 6837–6843.
Gale, W.F., and Totemeier, T.C. (2003) Smithells Metals Reference Book. Butterworth-Heinemann.
Goldschmidt, H.J. (1967) Carbides. Interstitial Alloys, 88–213. Springer.
Hazen, R.M., and Jeanloz, R. (1984) Wüstite ($Fe_{1-x}O$): A review of its defect structure and physical properties. Reviews of Geophysics, 22(1), 37–46.
Herbstein, F., and Snyman, J. (1964) Identification of Eckstrom-Adcock iron carbide as Fe_7C_3. Inorganic Chemistry, 3(6), 894–896.
Hillert, M., Höglund, L., and Ågren, J. (2005) Diffusion in interstitial compounds with thermal and stoichiometric defects. Journal of Applied Physics, 98(5), 053511.
Hull, A. (1917) Crystal structure of alpha-iron. Physical Review, 10, 661–696.
Kamada, S., Terasaki, H., Ohtani, E., Sakai, T., Kikegawa, T., Ohishi, Y., Hirao, N., Sata, N., and Kondo, T. (2010) Phase relationships of the Fe–FeS system in conditions up to the Earth's outer core. Earth and Planetary Science Letters, 294(1-2), 94–100.
Kamada, S., Ohtani, E., Terasaki, H., Sakai, T., Miyahara, M., Ohishi, Y., and Hirao,

N. (2012) Melting relationships in the Fe–Fe_3S system up to the outer core conditions. Earth and Planetary Science Letters, 359, 26–33.
Kaminsky, F.V., and Wirth, R. (2011) Iron carbide inclusions in lower-mantle diamond from Juina, Brazil. Canadian Mineralogist, 49(2), 555–572.
Koto, K., Morimoto, N., and Gyobu, A. (1975) The superstructure of the intermediate pyrrhotite. I. Partially disordered distribution of metal vacancy in the 6*C* type, $Fe_{11}S_{12}$. Acta Crystallographica, B31(12), 2759–2764.
Levchenko, E., Evteev, A., Belova, I., and Murch, G. (2009) Molecular dynamics simulation and theoretical analysis of carbon diffusion in cementite. Acta Materialia, 57(3), 846–853.
Li, J., Fei, Y., Mao, H., Hirose, K., and Shieh, S. (2001) Sulfur in the Earth's inner core. Earth and Planetary Science Letters, 193(3-4), 509–514.
Liu, J., Li, J., and Ikuta, D. (2016) Elastic softening in Fe_7C_3 with implications for Earth's deep carbon reservoirs. Journal of Geophysical Research: Solid Earth, 121(3), 1514–1524.
Machová, A., and Kadečková, S. (1977) Elastic constants of iron-silicon alloy single crystals. Czechoslovak Journal of Physics B, 27(5), 555–563.
Nakajima, Y., Takahashi, E., Sata, N., Nishihara, Y., Hirose, K., Funakoshi, K.-i., and Ohishi, Y. (2011) Thermoelastic property and high-pressure stability of Fe_7C_3: Implication for iron-carbide in the Earth's core. American Mineralogist, 96, 1158–1165.
Nakano, A., Tokonami, M., and Morimoto, N. (1979) Refinement of 3*C* pyrrhotite, Fe_7S_8. Acta Crystallographica, B35(3), 722–724.
Okamoto, H. (1992) The C-Fe (carbon-iron) system. Journal of Phase Equilibria, 13(5), 543–565.
Ozturk, B., Fearing, V., Ruth, J., and Simkovich, G. (1984) The diffusion coefficient of carbon in cementite, Fe_3C, at 450 °C. Solid State Ionics, 12, 145–151.
Palache, C., Berman, H., and Frondel, C. (1944) The System of Mineralogy of James Dwight Dana and Edward Salisbury Dana, vol. I—elements, sulfides, sulfosalts and oxides. Wiley.
Pauling, L. (1960) The Nature of the Chemical Bond. Cornell University Press, Ithaca, New York.
Petch, N. (1944) The interpretation of the crystal structure of cementite. Journal of the Iron and Steel Institute, 149, 143–150.
Prescher, C., and Prakapenka, V.B. (2015) DIOPTAS: a program for reduction of two-dimensional X-ray diffraction data and data exploration. High Pressure Research, 35(3), 223–230.
Prescher, C., Dubrovinsky, L., Bykova, E., Kupenko, I., Glazyrin, K., Kantor, A., McCammon, C., Mookherjee, M., Nakajima, Y., and Miyajima, N. (2015) High Poisson's ratio of Earth's inner core explained by carbon alloying. Nature Geoscience, 8(3), 220.
Rohrbach, A., and Schmidt, M.W. (2011) Redox freezing and melting in the Earth's deep mantle resulting from carbon-iron redox coupling. Nature, 472, 209–212.
Routbort, J., Reid, C., Fisher, E., and Dever, D. (1971) High-temperature elastic constants and the phase stability of silicon-iron. Acta Metallurgica, 19(12), 1307–1316.
Scott, H.P., Williams, Q., and Knittle, E. (2001) Stability and equation of state of Fe_3C to 73 GPa: Implications for carbon in the Earth's core. Geophysical Research Letters, 28(9), 1875–1878.
Seto, Y., Nishio-Hamane, D., Nagai, T., and Sata, N. (2010) Development of a software suite on X-ray diffraction experiments. Review of High Pressure Science and Technology, 20(3).
Smith, E.M., Shirey, S.B., Nestola, F., Bullock, E.S., Wang, J., Richardson, S.H., and Wang, W. (2016) Large gem diamonds from metallic liquid in Earth's deep mantle. Science, 354, 1403–1405.
Walker, D., Dasgupta, R., Li, J., and Buono, A. (2013) Nonstoichiometry and growth of some Fe carbides. Contributions to Mineralogy and Petrology, 166(3), 935–957.
Walker, D., Li, J., Kalkan, B., and Clark, S.M. (2015) Thermal, compositional, and compressional demagnetization of cementite. American Mineralogist, 100, 2610–2624.

Manuscript received June 5, 2018
Manuscript accepted November 9, 2018
Manuscript handled by Ryosuke Sinmyo